British Journal of Cancer www.nature.com/bjc

ARTICLE

Translational Therapeutics

Biparatopic anti-HER2 drug radioconjugates as breast cancer theranostics

Jessica Pougoue Ketchemen[1], Hanan Babeker[1,2], Anjong Florence Tikum[1], Anand Krishnan Nambisan[1], Fabrice Ngoh Njotu[1], Emmanuel Nwangele[1] and Humphrey Fonge[1,3]✉

© Crown 2023

BACKGROUND: HER2 is overexpressed in 25–30% of breast cancer. Multiple domains targeting of a receptor can have synergistic/additive therapeutic effects.

METHODS: Two domain-specific ADCs trastuzumab-PEG$_6$-DM1 (domain IV) and pertuzumab-PEG$_6$-DM1 (domain II) were developed, characterised and radiolabeled to obtain [^{89}Zr]Zr-trastuzumab-PEG$_6$-DM1 and [^{67}Cu]Cu-pertuzumab-PEG$_6$-DM1 to study their in vitro (binding assay, internalisation and cytotoxicity) and in vivo (pharmacokinetics, biodistribution and immunoPET/SPECT imaging) characteristics.

RESULTS: The ADCs had an average drug-to-antibody ratio of 3. Trastuzumab did not compete with [^{67}Cu]Cu-pertuzumab-PEG$_6$-DM1 for binding to HER2. The highest antibody internalisation was observed with the combination of ADCs in BT-474 cells compared with single antibodies or ADCs. The combination of the two ADCs had the lowest IC$_{50}$ compared with treatment using the single ADCs or controls. Pharmacokinetics showed biphasic half-lives with fast distribution and slow elimination, and an AUC that was five-fold higher for [^{89}Zr]Zr-trastuzumab-PEG$_6$-DM1 compared with [^{67}Cu]Cu-pertuzumab-PEG$_6$-DM1. Tumour uptake of [^{89}Zr]Zr-trastuzumab-PEG$_6$-DM1 was 51.3 ± 17.3% IA/g (BT-474), and 12.9 ± 2.1% IA/g (JIMT-1) which was similarly to [^{67}Cu]Cu-pertuzumab-PEG$_6$-DM1. Mice pre-blocked with pertuzumab had [^{89}Zr]Zr-trastuzumab-PEG$_6$-DM1 tumour uptakes of 66.3 ± 33.9% IA/g (BT-474) and 25.3 ± 4.9% IA/g (JIMT-1) at 120 h p.i.

CONCLUSION: Using these biologics simultaneously as biparatopic theranostic agents has additive benefits.

British Journal of Cancer; https://doi.org/10.1038/s41416-023-02272-4

INTRODUCTION

Breast cancer is the most common cancer and the second leading cause of cancer death in women [1]. Human epidermal growth factor receptor II (HER2) is amplified and overexpressed in 25–30% of breast cancer (BC), and it is particularly associated with disease aggressiveness, poor diagnosis, and poor overall survival (OS) [2]. Trastuzumab, pertuzumab, lapatinib, trastuzumab emtansine (T-DM1) and trastuzumab deruxtecan (T-DXd) are approved agents for treating HER2 positive BC [3]. Despite great improvements in patients' outcomes over the last decade using these anti-HER2 agents, resistance is common. Trastuzumab in combination with taxanes or anthracyclines shows improved efficacy and survival benefits in HER2-positive BC [4, 5]. However, up to 70% of patients selected for trastuzumab do not respond or acquire resistance to the drug [6, 7]. Combination of pertuzumab (domain-II binder) and trastuzumab (domain-IV binder) is approved for treating HER2-positive BC [8, 9]. Several preclinical studies show that the combination of pertuzumab and trastuzumab is superior compared with their single agents against HER2-positive models [10–12]. Trastuzumab antibody drug conjugate (ADC) in which the antibody is conjugated to potent cytotoxic agent maytansine (DM1) (trastuzumab-DMI (T-DM1)), has shown efficacy in patients with HER2-positive trastuzumab- or lapatinib-resistant phenotypes and has been approved [13]. Despite the potency of T-DM1 clinical overall response rate (ORR) is a modest 35% [14, 15] and resistance to this and other ADCs is widespread [16, 17]. Intra-tumoral heterogeneity of target expression is another critical factor that causes variability in response to antibody therapeutics and hence resistance. Membrane permeable drugs such as monomethyl auristatin E (MMAE) can diffuse from targeted cells to neighbouring cancer cells causing toxicity using the 'bystander effect' [18] to kill resistant cells that do not have sufficient expression of antigen. Bystander effect is a key attribute accounting for the enhanced effectiveness of T-DXd over T-DM1 in HER2-positive cancers [19–21]. Despite these advances, novel strategies are required to overcome resistances mechanisms and increase progression-free survival (PFS) and OS of patients with HER2-positive BC.

Several strategies have been investigated to improve the effectiveness of HER2-targeted monoclonal antibodies (mAbs) including the use of bispecific and biparatopic immunoconjugates.

[1]Department of Medical Imaging, College of Medicine, University of Saskatchewan, Saskatoon, SK S7N 0W8, Canada. [2]Department of Pathology and Lab. Medicine, College of Medicine, University of Saskatchewan, 107 Wiggins Rd, Saskatoon, SK S7N 5A2, Canada. [3]Department of Medical Imaging, Royal University Hospital Saskatoon, SK, Saskatoon, SK S7N 0W8, Canada. ✉email: humphrey.fonge@usask.ca

Received: 20 October 2022 Revised: 30 March 2023 Accepted: 5 April 2023
Published online: 24 April 2023

Biparatopic targeting (more than one epitope or domain of an antigen using one or more antibodies) of antigens on cancer cells using antibodies enhances tumour cell clustering, receptor internalisation and has shown some promise preclinically. Novel promising anti-HER2 biparatopic and bispecific antibodies including ZY49 and ZW25 are in different phases of development [22–24]. Li et al. [22] showed that an anti-HER2 biparatopic monoclonal antibody promoted robust internalisation, lysosomal trafficking, and degradation. When conjugated with a tubulysin-based microtubule inhibitor, the biparatopic ADC demonstrated superior anti-tumour activity compared with T-DM1 in tumour models including in situations where T-DM1 would be ineligible and refractory to the drug [22].

DM1 is an anti-microtubule agent that is used in many ADCs in clinical development. A major cause of resistance to ADCs is the expression of drug efflux by multidrug-resistant (MDR1) pumps [16, 17]. Like most small-molecule chemotherapeutic agents, DM1 is an MDR1 substrate, however, PEGylated DM1 (PEG-DM1), as proposed in this study, has the same potency as DM1 but is not a substrate for MDR1 [25, 26]. Pertuzumab (domain-II specific) and trastuzumab (domain-IV specific) bind to different domains of HER2 and a combination of both is approved for treating HER2-positive BC [8, 9].

Radiolabeling of ADCs is emerging as a powerful tool to understand the in vivo pharmacology of these immunoconjugates. Zirconium-89 (^{89}Zr) is an appropriate positron emission tomography (PET) isotope for antibodies because of its half-life (78.4 h) that approximates that of most antibodies [27]. In addition, its residualizing characteristics ensures enhanced tumour retention leading to good tumour-to-normal tissue ratios, and overall image quality. Copper-67 (^{67}Cu) with a half-life of 61.8 h is another appropriate single photon emission computed tomography (SPECT) isotope with radiotherapeutic properties [28]. The 100% beta emission of ^{67}Cu can be exploited for radiotherapy, and its high gamma branching ratio makes it suitable for SPECT imaging. For years, ^{67}Cu was limited in supply but recent developments in the field have allowed researchers to produce large quantities of ^{67}Cu with high radionuclidic purity [29].

To design effective therapies against HER2-positive BC, we propose to develop ADCs that target different domains/epitopes of HER2 that are not MDR substrates using PEG$_6$-DM1. In this work, we developed for the first time pertuzumab-PEG$_6$-DM1 and trastuzumab-PEG$_6$-DM1 ADCs as anti-HER2 biparatopic immunoconjugates. To understand their in vitro and in vivo behaviour, we then developed [^{67}Cu]Cu-pertuzumab-PEG$_6$-DM1 and [^{89}Zr]Zr-trastuzumab-PEG$_6$-DM1. Our overall objective was to characterise the in vitro binding, two dimensional in vitro cytotoxicity and in vivo distribution of simultaneous administration of the ADCs to evaluate their properties that could indicate their future therapeutic effectiveness.

MATERIALS AND METHODS

Cell lines, reagents and xenografts

Human breast cancer cell lines (BT-474 (RRID:CVCL_0179) and SKBR3 (RRID:CVCL_0033)), JIMT-1 (RRID:CVCL_2077), and MCF-7 (RRID:CVCL_0031) with high, medium and low HER2 expression, respectively, were purchased from American Type Culture Collection (ATCC) (Rockville, MD). These cells were cultured in monolayers by serial passages in their various media and the media was supplemented with 10% foetal bovine serum (FBS) (Biochrom, Sigma-Aldrich, St Louis, MO) and 1% penicillin–streptomycin (Hyclone Laboratories, Logan, UT) at 37 °C in a humidified atmosphere with 5% carbon dioxide (CO_2). BT-474 was cultured in Hybri-Care medium (catalogue # 46-X), supplemented with 1.5 g/L sodium carbonate. JIMT-1 and SKBR3 were cultured in high glucose Dulbecco's Modified Eagle's medium (DMEM) (Hyclone Laboratories, Logan, UT) and MCF-7 was propagated in Eagle's Minimum Essential medium (EMEM). All cell lines were authenticated using short tandem repeat (STR) profiling at the Centre for Applied Genomics (Hospital for SickKids, Toronto, ON). Cells were free of mycoplasma prior to use.

Clinical-grade monoclonal antibodies T-DM1, trastuzumab, pertuzumab, and control human antibody anti-CD20 (rituximab) were generously provided by the Saskatchewan Cancer Agency (SCA, Saskatoon, SK). Maytansine (DM1) was obtained from Toronto Research Chemicals, and NHS-PEG$_6$-maleimide from Biochempeg (Watertown, MA).

Female athymic Balb-C nude mice ($n = 3$–4/group with tumour volume of 60–170 mm^3 body weights of 20–22 g) were used for biodistribution studies, and imaging experiments were carried out using female athymic CD-1 nude mice ($n = 2$/group with tumour volume of 60–170 mm^3 and body weights of 20–22 g). All mice used were at least four weeks of age and purchased from Charles River (Saint-Constant, QC). These mice were approved, supervised, and maintained following the guidelines set for by the University of Saskatchewan Animal Care Committee (UACC) (protocols # 20170084 and 20220021). The animals were maintained in specific conditions, such as 12 h light and 12 dark cycles, temperature, and humidity-controlled vivarium, and had ad libitum access to food (Lab Diet, St. Louis, MO) and water. After a minimum of one week of acclimatisation, athymic CD-1 nude mice and athymic Balb/C nude mice were inoculated with 17-β-estradiol pellets (0.36 mg-1.7 mg/pellet, 90-day sustained release) from Innovative Research of America, Sarasota, FL, US). Each mouse received a pellet at the left back around the neck region 72–120 h before inoculating the tumour cell lines [30]. The subcutaneous injection was done with 10–20 million cells of BT-474, and JIMT-1 in 100 µL suspension of a 1:1 mixture of complete growth media and Matrigel matrix basement membrane (Discovery Laboware, Inc. Bedford, MA). Two groups of mice (CD-1 nude mice, and athymic Balb/C nude mice) were inoculated with BT-474 and JIMT-1 cells on the right and left thigh of the hind leg, respectively. The mice were monitored daily, and tumour growth was determined using a digital caliper. Second and third injections of cells were done when necessary to obtain the required tumour volume. All animals used were at least 6 weeks of age.

Synthesis of ADCs and conjugation with bifunctional chelators

The ADCs trastuzumab-PEG$_6$-DM1, pertuzumab-PEG$_6$-DM1 and control IgG rituximab-PEG$_6$-DM1 with ~3 drug to antibody ratio (DAR) were synthesised following SOPs published by our group [31, 32]. An 8-mole excess of a 20 mg/mL of DM1-PEG$_6$-NHS in DMSO solution was incubated with the unconjugated antibodies for 2 h at 37 °C and then for 18–20 h at 4 °C. The reaction mixture was maintained on a shaker. The DAR was confirmed using nanodrop-ultraviolet (UV) spectrophotometry at two wavelengths (254 nm and 280 nm) [33] and the molecular weights (in triplicates). Molecular weight and purity determination was performed using an Agilent 2100 Bioanalyzer system (Agilent High Sensitivity Protein 250 Kit- cat# 5067–1575) following the manufacturer's protocol. Size-exclusion HPLC (SEC-HPLC) was performed using a Waters 2796 Bioseparations Module, Waters 2487 Dual λ Absorbance Detector, XBridge® BEH 200 A SEC 3.5 µm 7.8 × 150 nm column (Waters Corporation, Milford, MA) to further confirmed the purity and integrity of each ADC. The UV-detector was fixed at 254 nm and 280 nm, and PBS was used as mobile phase at a flow rate of 0.45 mL/min.

For radiolabeling with ^{89}Zr, trastuzumab-PEG$_6$-DM1 and rituximab-PEG$_6$-DM1 were conjugated with *p*-isothiocyanatobenzyl desferrioxamine (*p*-SCN-Bz-DFO, Macrocyclics, Plano TX) to obtain DFO-trastuzumab-PEG$_6$-DM1 and DFO-rituximab-PEG$_6$-DM1 following lab SOPs [34]. Similarly, pertuzumab-PEG$_6$-DM1 was conjugated with *p*-SCN-Bz-DOTA (Macrocyclic, Plano TX) to obtain DOTA-pertuzumab-PEG$_6$-DM1 to allow for radiolabeling with ^{67}Cu using lab SOPs [31]. A 15-mole excess of either *p*-SCN-Bz-DFO or *p*-SCN-Bz-DOTA in DMSO was added to the respective ADCs solutions and incubated at 37 °C on a shaker for 90 min (making sure that the reaction mixture contained less than 5% of DMSO). The molecular weight and purity determinations were performed as described above.

Binding kinetics and flow cytometry

To determine the binding kinetics in BT-474, SKBR3, JIMT-1 and MCF-7 cell lines, cells were first treated with naked antibodies, ADCs and ADCs conjugated with bifunctional chelators, at different concentrations (4–12 points following threefold serial dilutions) in triplicates using lab SOPs [34]. Cells were first collected and washed with PBS, and the antibodies were serially diluted starting with 2 µM. The cells were incubated with the respective antibodies for 30 min at 4 °C followed by a second wash with PBS, prior to their suspension in a 1:100 dilution PE labelled Secondary Antibody, Goat Anti-Human IgG Fc (cat# 12-4998-82). Suspended cells

were incubated as described above, washed, and resuspended in 200 µL PBS before analysis using a flow cytometer. Flow cytometry data were acquired using CytoFLEX (Beckman Coulter) and analysed using FlowJo (version 10.7.2; FlowJo LLC). GraphPad Prism Version 9 (GraphPad Software) was used to determine the binding constant (K_D) and half maximal effective concentration (EC_{50}).

Radiolabeling and characterisation of radioimmunoconjugates

^{89}Zr-oxalate and ^{67}Cu-chloride were produced at the Saskatchewan Cyclotron Facility University of Saskatchewan (Saskatoon, SK) and Canadian Isotope Innovations Corp (CIIC, Saskatoon, SK), respectively. ^{89}Zr radiolabeling was accomplished following standard laboratory protocol using a specific activity of 1 MBq/2 µg [35]. ^{67}Cu radiolabeling was carried out by adding 150 mM ammonium acetate buffer to $^{67}CuCl_2$ solution, pH was maintained at 5.8–6, and incubation was done for 30 min at 37 °C using a specific activity of 1 MB/1 µg [29]. Following radiolabeling, the reaction mixture was cooled to room temperature, and radiochemical yield and purity was determined using instant thin layer chromatography (iTLC) with 100 nM sodium citrate buffer (pH 5.0) as mobile phase. Radiochemical purity and radiolabeling efficiency were also determined using SEC-HPLC as described above. The antibody drug radioconjugates (ADRs) were formulated in PBS. Radiochemical purity of 92–95% was used for in vitro and in vivo experiments [36].

In vitro saturation and competitive binding

BT-474 cells were used to evaluate the in vitro saturation binding of [^{67}Cu]Cu-pertuzumab-PEG$_6$-DM1 and [^{89}Zr]-trastuzumab-PEG$_6$-DM1, as well as the domain-specific binding (competitive binding). To determine the in vitro saturation binding, 5×10^5 cells in PBS were added in 1.5 mL Eppendorf tubes and incubated with increasing concentrations of each labelled antibody (0.09–50 nM in 100 µL PBS) for 4 h at 4 °C (total binding). For nonspecific binding (NSB), a 100-fold molar excess (with respect to the highest concentration) of unlabelled antibody DOTA-pertuzumab-PEG$_6$-DM1 was added to another group of cells and incubated for 2 h at 4 °C prior to the addition of the radiolabeled conjugate. The K_D was obtained using a non-linear regression curve and one-site binding equation on GraphPad Prism Version 9 (GraphPad Software, La Jolla, CA).

For competitive binding, a 100-fold molar excess of naked trastuzumab was introduced in a third set of vials containing 5×10^5 cells, incubated for 2 h at 4 °C and then for 4 h at 4 °C after [^{67}Cu]Cu-pertuzumab-PEG$_6$-DM1 was added. Each group of cells (in triplicates) were washed three times with PBS, and centrifuged at 161 g to collect the supernatant. The pellet and the respective supernatants were measured using the gamma counter (Wallac Wizard 1480, PerkinElmer, Waltham, MA) [36]. Total, NSB and specific binding were used to determine the K_D and the binding potential (B_{max}) were evaluated using GraphPad Prism Version 9.

Internalisation of immunoconjugates

BT-474 and MCF-7 cells (10,000 per well) were plated on two flat-bottom 96-well plates and incubated for 48 h prior to the addition of the immunoconjugates. Trastuzumab, trastuzumab-PEG$_6$-DM1, pertuzumab, pertuzumab-PEG$_6$-DM1, combination of trastuzumab-PEG$_6$-DM1 and pertuzumab-PEG$_6$-DM1, rituximab and rituximab-PEG$_6$-DM1 at a concentration of 24.6 nM were mixed with the IncuCyte® FabFluor reagent (Essen BioScience, Ann Arbor, MI) at a molar ratio of 1:3 in complete growth media and incubated for 15 min at 37 °C. To the cells (in triplicates) were added 50 µL of complete growth media, followed by 50 µL of the FabFluor-labelled antibody, and immediately placed in the IncuCyte® S3 live-cell imager (Essen BioScience, Ann Arbor, MI) where images were captured every 2 h for 48 h. The area under the curve (AUC (µm^2 h)) was calculated from the red object area versus time curve and was used to quantify and compare the extent of internalisation of the immunoconjugates using GraphPad Prism Version 9.

In vitro cytotoxicity of ADCs

The in vitro cytotoxicity of T-DM1, trastuzumab-PEG$_6$-DM1, pertuzumab-PEG$_6$-DM1 and the (1:1) combination of trastuzumab-PEG$_6$-DM1 + pertuzumab-PEG$_6$-DM1 was determined using IncuCyte® S3 live-cell imaging system in BT-474, SKBR3, JIMT-1, and MCF-7 cell lines. The cells were harvested and seeded into a 96-well clear flat-bottom plate pre-coated with poly-D-lysine Corning plates (10,000 cells in 200 µL per well) 48 h prior to the treatment. After 48 h, the culture media was removed, and the cells were then treated with different concentrations (10 serial dilutions from 2000 to 0.1 nM of T-DM1, trastuzumab-PEG$_6$-DM1, pertuzumab-PEG$_6$-DM1 and the combination of ADCs (trastuzumab-PEG$_6$-DM1 + pertuzumab-PEG$_6$-DM1, all in triplicates) in complete growth media containing IncuCyte® Cytotox Red reagent and incubated at 37 °C for 30 min before imaging. Live-cell images were captured every 2 h using a ×10 objective lens using phase contrast and fluorescence channel. During each scanning, four images were acquired for each of the wells until the end of the experiment. The fluorescence red count generated was used to calculate the IC_{50} values using GraphPad Prism Version 9.

In vitro stability

The in vitro stability of [^{67}Cu]Cu-pertuzumab-PEG$_6$-DM1 and [^{89}Zr]Zr-trastuzumab-PEG$_6$-DM1 was determined in PBS and in human serum at 37 °C for 5 days ($n = 3$). Each antibody drug radioconjugate (ADR) was incubated at the respective incubation conditions to make a final concentration of 8–10 MBq/300 µL. To analyse the purity, 10 µL (triplicates) of each ADR was drawn for iTLC [37].

Pharmacokinetics

The pharmacokinetics of [^{67}Cu]Cu-pertuzumab-PEG$_6$-DM1 and [^{89}Zr]Zr-trastuzumab-PEG$_6$-DM1 were studied in normal Balb/C mice ($n = 3$/group). In total, 5 MBq of the radioimmunoconjugates in saline was injected intravenously via a tail vein, and blood were collected at different time points (0.083–120 h) in heparinized capillary tubes. The samples were counted using a gamma counter, and radioactivity in blood was calculated as the percentage of injected activity/mL (% IA/mL). The volume of distribution at steady state (Vss), elimination half-life, distribution, area under the curve (AUC), and clearance (CL) pharmacokinetics parameters were obtained by fitting a curve of blood radioactivity versus time to a two-compartment model with intravenous bolus input.

ImmunoPET/CT, immunoSPECT/CT imaging and biodistribution

For imaging studies, CD-1 nude mice ($n = 2$/group) bearing BT-474 (high HER2 expression), and JIMT-1 (medium HER2 expression) tumour xenografts were injected via a tail vein with [^{67}Cu]Cu-pertuzumab-PEG$_6$-DM1 or [^{89}Zr]Zr-trastuzumab-PEG$_6$-DM1. A group of mice received 10 MBq/20 µg of [^{89}Zr]Zr-trastuzumab-PEG$_6$-DM1 followed by microPET/CT, and another group received 10 MBq/10 µg of [^{67}Cu]Cu-pertuzumab-PEG$_6$-DM1 followed by microSPECT/CT. The control group was injected with [^{89}Zr]Zr-rituximab-PEG$_6$-DM1. Biparatopic imaging was studied in a group of mice following a tail vein injection with 10 MBq of a 1:1 mixture of [^{67}Cu]Cu-pertuzumab-PEG$_6$-DM1 and [^{89}Zr]Zr-trastuzumab-PEG$_6$-DM1. Imaging studies were performed at 24 h, 48 h and 120 h post injection (p.i.) using the Vector^{4}CT scanner (MILabs B.V., Utrecht, The Netherlands). PET and SPECT scans were acquired in a list-mode data format using a high-energy ultra-high resolution (HE-UHR-1.0 mm) mouse/rat pinhole collimator, while the CT scans were obtained using a pixel-based order-subset expectation maximisation (POS-EM) algorithm.

Biodistribution was studied in athymic Balb/C nude mice bearing BT-474 and JIMT-1 tumours at 24 h and 120 h p.i. Groups of mice ($n = 3$–4/group) were injected with [^{89}Zr]Zr-trastuzumab-PEG$_6$-DM1, [^{67}Cu]Cu-pertuzumab-PEG$_6$-DM1, and control [^{89}Zr]Zr-rituximab-PEG$_6$-DM1 as described in the imaging studies above. For domain-specific tumour uptake, a group of mice received [^{89}Zr]Zr-trastuzumab-PEG$_6$-DM1 with 500 µg of pertuzumab. Organs were weighed, counted for activity and tissue uptake was expressed as % IA/g [37]. For all animal studies, no blinding was done.

Statistical analysis

All data were expressed as the mean +/− standard error of the mean (SEM). A one-way ANOVA, and two-way ANOVA with Bonferroni post hoc test was used to determine the statistical significance between groups. All graphs were analysed using GraphPad Prism Version 9 (GraphPad software).

RESULTS

Conjugation and QC of immunoconjugates

The conjugation of trastuzumab, pertuzumab and rituximab with PEG$_6$-NHS-DM1 allowed us to produce ADCs with a drug-to-antibody ratio (DAR) of ~3 for all the ADCs confirmed by the bioanalyzer and the nanodrop UV–Vis spectrophotometry. These

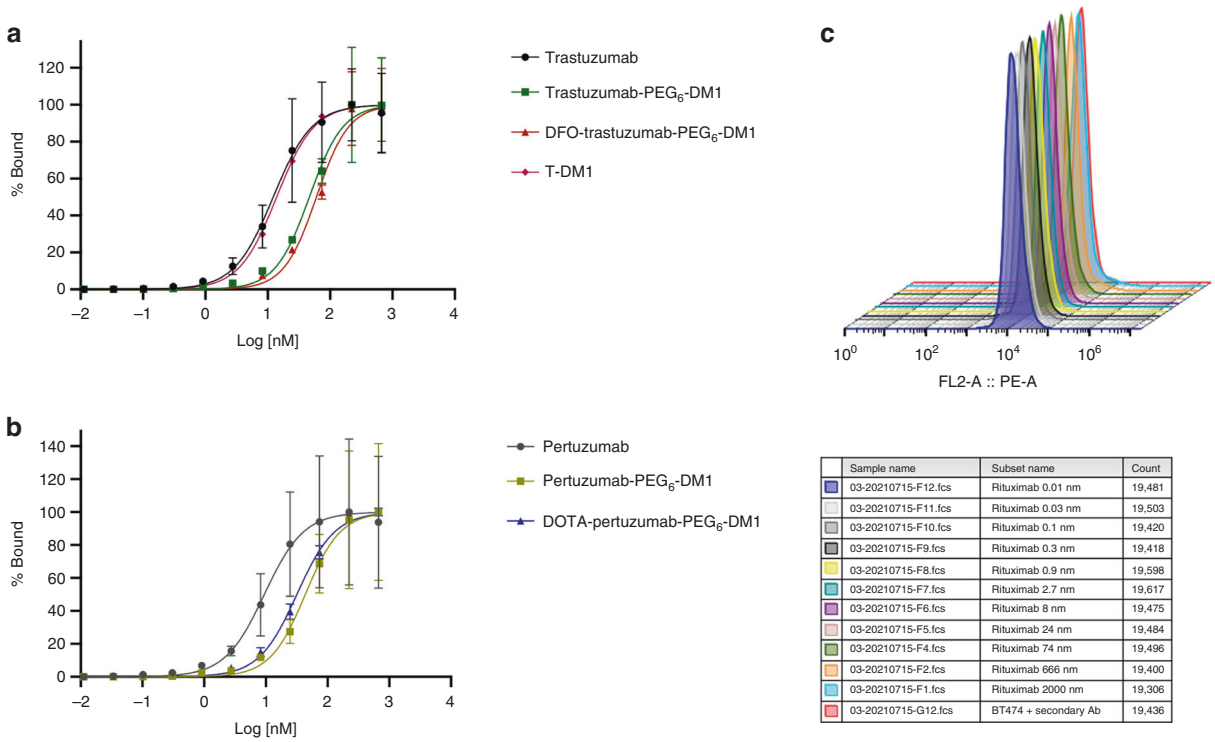

Fig. 1 Flow cytometry saturation binding assay of antibodies and immunoconjugates in HER2-positive BT-474 cells. a Trastuzumab, trastuzumab-PEG$_6$-DM1, DFO-trastuzumab-PEG$_6$-DM1 and T-DM1. **b** Pertuzumab, pertuzumab-PEG$_6$-DM1 and DOTA-pertuzumab-PEG$_6$-DM1, and **c** three-dimensional flow cytometry histograms of isotype control antibody rituximab.

Table 1. K_D and EC_{50} of antibodies and ADCs compared with T-DM1 in BT-474 cells.

Antibody/immunoconjugate	K_D (nM)	EC_{50} (nM)	B_{max}
Trastuzumab	13.3 ± 2.5	12.3 ± 1.6	7517834 ± 299992.3
Trastuzumab-PEG$_6$-DM1	63.4 ± 11.5	46.5 ± 4.9	7463698 ± 376770.8.
DFO-trastuzumab-PEG$_6$-DM1	86.9 ± 11.3	60.3 ± 4.4	7294157 ± 291972.6
T-DM1	15.7 ± 0.5	13.9 ± 0.1	6296868 ± 49738.7
Pertuzumab	9.9 ± 3.1	9.4 ± 2.1	6668215 ± 387531.7
Pertuzumab-PEG$_6$-DM1	57.3 ± 15.4	43.5 ± 6.6	7177197 ± 493389.2
DOTA-pertuzumab-PEG$_6$-DM1	40.1 ± 1.6	31.8 ± 0.7	3892336 ± 42612.5

ADCs were then conjugated with DFO for trastuzumab-PEG$_6$-DM1 and rituximab-PEG$_6$-DM1, and DOTA for pertuzumab-PEG$_6$-DM1 to allow for the radiolabeling with ^{89}Zr, and ^{67}Cu, respectively (Supplementary Fig. 1A). HPLC showed that DFO or DOTA-conjugated ADCs were ~98% pure with less than 2% aggregates or degradation. Bioanalyzer experiments further confirmed the purity as well as the molecular weight of the different immunoconjugates (Supplementary Fig. 1B, C). This also allowed for the calculation of the DAR (Supplementary Table 1).

Flow cytometry of antibodies and immunoconjugates

Flow cytometry was used to determine the in vitro binding of the different immunoconjugates in BT-474, SKBR3, JIMT-1 and MCF-7. We observed a concentration-dependent binding of the immunoconjugates with these cell lines with little to no binding to the control antibody conjugate (rituximab), as shown by the mean fluorescent intensity (MFI) values (Fig. 1). To calculate the binding constants, K_D, and EC_{50} of the different immunoconjugates, a saturation binding curve of percentage bound against concentration was plotted. K_D values of ADCs were determined and compared with unconjugated antibodies and T-DM1 for BT-474 (Fig. 1 and Table 1), and for JIMT-1, SKBR3 and MCF-7 (Supplementary Fig. 2 and Supplementary Table 2). Three-dimensional histograms of flow cytometry is presented (Supplementary Fig. 3A–H). The K_D of trastuzumab (13.3 ± 2.5 nM) was lower than the ADC trastuzumab-PEG$_6$-DM1 (63.4 ± 11.5 nM), which was not significantly different ($P < 0.05$) from the DFO-conjugated ADC DFO-trastuzumab-PEG$_6$-DM1 (86.9 ± 11.3 nM). In comparison, the K_D of T-DM1 was 15.7 ± 0.5 was lower but not significantly different. Similar trend was observed for pertuzumab, and in all cell lines. This indicates conjugation of the drug decreased the binding to HER2 (Table 1).

Saturation and competitive radioligand binding

All radioimmunoconjugates had radiochemical yields of more than 95% as confirmed by iTLC and SEC-HPLC (Supplementary Fig. 4). Saturation radioligand binding assay was studied in BT-474 cell line to determine if conjugation and radiolabeling affected the radioimmunoconjugates. The K_D (B_{max}) of [^{67}Cu]Cu-pertuzumab-PEG$_6$-DM1 and [^{89}Zr]Zr-trastuzumab-PEG$_6$-DM1 was 11.5 ± 0.9 nM (B_{max} 2831708 ± 94410.7) and 13.5 ± 0.8 nM (B_{max} 1074108 ± 24343.2), respectively (Fig. 2a, b).

Competitive binding using trastuzumab (domain IV) was performed to confirm the domain-specific binding of [^{67}Cu]Cu-

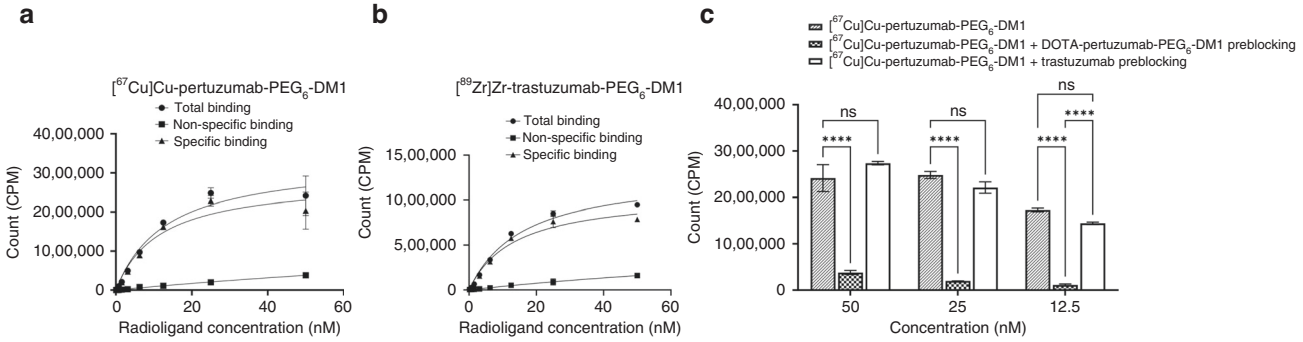

Fig. 2 Radioligand and competitive binding assays in HER2-positive BT-474 cells. a Radioligand binding assay of [^{67}Cu]Cu-pertuzumab-PEG$_6$-DM1 showing total, nonspecific and specific binding. **b** Radioligand binding assay of [^{89}Zr]Zr-trastuzumab-PEG$_6$-DM1 showing total, nonspecific and specific binding. The specific binding was calculated by subtracting the nonspecific binding from total binding. **c** Competitive binding of unlabelled trastuzumab and [^{67}Cu]Cu-pertuzumab-PEG$_6$-DM1 at different concentrations, indicating domain specificity to HER2 of pertuzumab and trastuzumab.

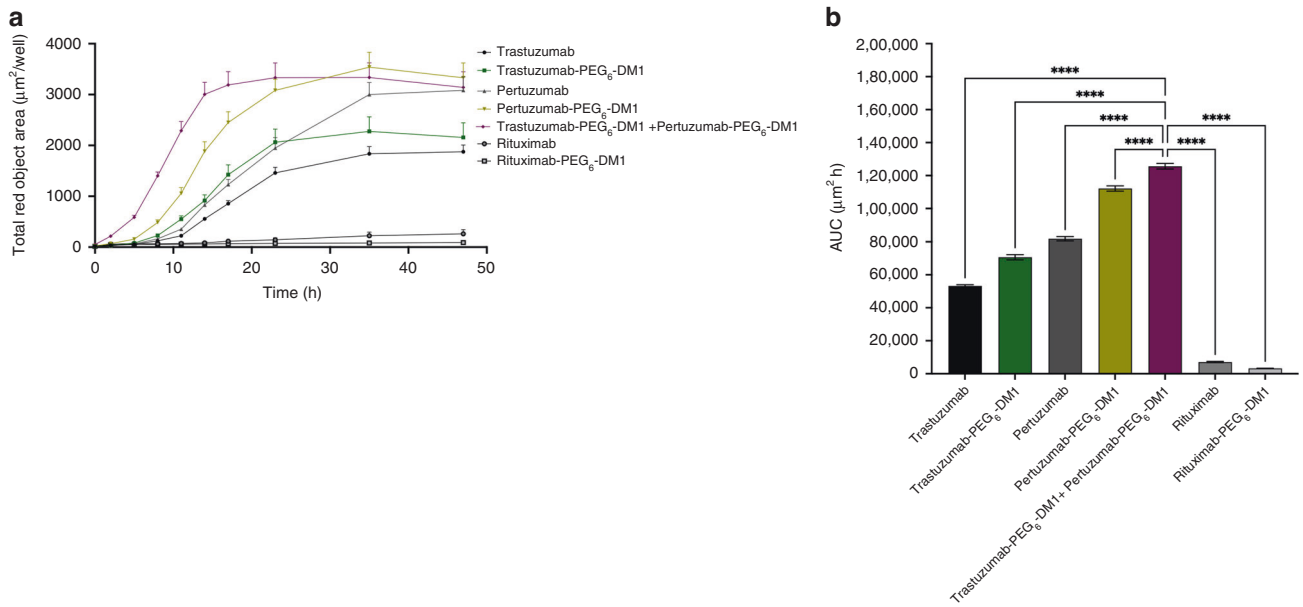

Fig. 3 Antibody internalisation of trastuzumab, trastuzumab-PEG$_6$-DM1, pertuzumab, pertuzumab-PEG$_6$-DM1 and a combination of trastuzumab-PEG$_6$-DM1 + pertuzumab-PEG$_6$-DM1 in HER2-positive BT-474 cell line after 48 h of incubation. Rituximab and its conjugate were used as controls. **a** Internalisation of antibodies was studied using Incucyte live-cell imaging in BT-474 cell line. Internalisation of all antibodies and immunoconjugates peaked at 12–22 h post incubation, and remained saturated over the study period—48 h. **b** The extent of internalisation is represented as the AUC (area under the curve) plotted using GraphPad Prism Version 9. Statistical significance of the extent of internalisation of different treatments compared with biparatopic treatment of pertuzumab-PEG$_6$-DM1 + trastuzumab-PEG$_6$-DM1 was analysed using *t* test with **** indicating statistical significance ($P < 0.0001$).

pertuzumab-PEG$_6$-DM1 to domain II of HER2. [^{67}Cu]Cu-pertuzumab-PEG$_6$-DM1 bound specifically to domain II. There was no binding in the presence of cold DOTA-pertuzumab-PEG$_6$-DM1 ($P < 0.0001$), while in the presence of trastuzumab there was no reduction in the binding, confirming the domain specificity of [^{67}Cu]Cu-pertuzumab-PEG$_6$-DM1 (Fig. 2c).

Internalisation and in vitro cytotoxicity of immunoconjugates

In BT-474 cells, a rapid time-dependent increase in red fluorescence (internalisation immunoconjugates into the lysosomes and endosomes) was observed for trastuzumab and pertuzumab conjugates from 2 to 48 h, with the highest fluorescence observed with the simultaneous addition of trastuzumab-PEG$_6$-DM1 and pertuzumab-PEG$_6$-DM1. Internalisation was dependent on receptor density and was far greater for BT-474 compared with MCF-7 (Fig. 3a, b, Table 2 and

Table 2. Area under the curve (AUC) of internalised antibodies and ADCs with HER2-positive BT-474 cells studied over 48-h incubation period and plotted using GraphPad Prism Version 9.

Construct	AUC (µm^2 h) ± SEM
Trastuzumab	53229 ± 1289.3
Trastuzumab-PEG$_6$-DM1	70647 ± 2765.9
Pertuzumab	81882 ± 2298.5
Pertuzumab-PEG$_6$-DM1	112142 ± 2742.6
Trastuzumab-PEG$_6$-DM1 + pertuzumab-PEG$_6$-DM1	125647 ± 2980.7
Rituximab	7096 ± 670.9
Rituximab-PEG$_6$-DM1	3275 ± 107.1

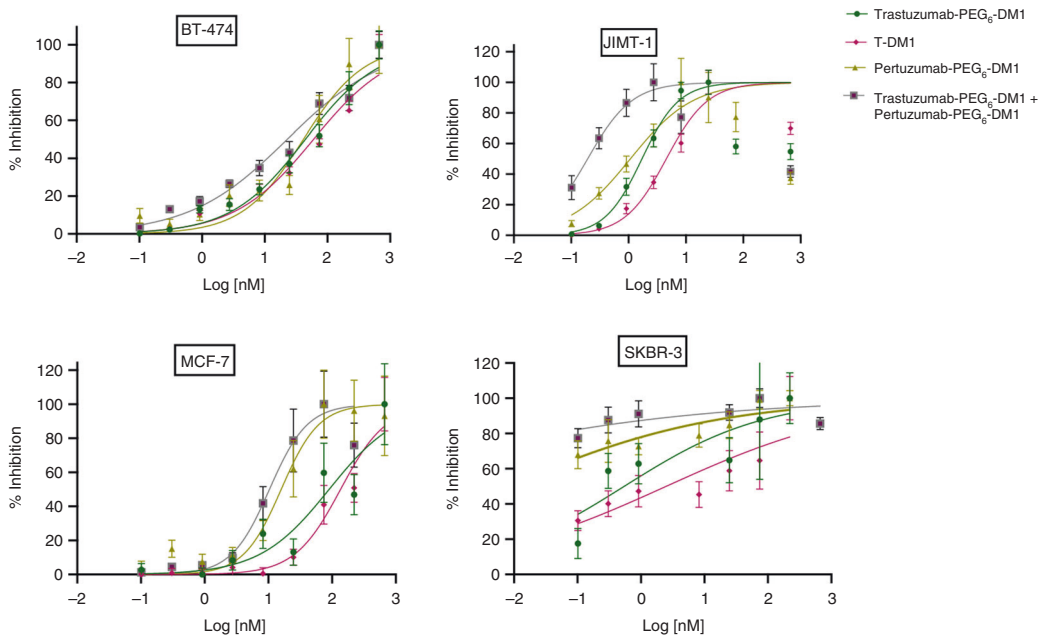

Fig. 4 In vitro cytotoxicity of immunoconjugates in cells with different HER2 densities. Cytotoxicity of trastuzumab-PEG$_6$-DM1, T-DM1 and pertuzumab-PEG$_6$-DM1 as well as biparatopic combination trastuzumab-PEG$_6$-DM1 + pertuzumab-PEG$_6$-DM1 in HER2-positive breast cancer cell lines with high (BT-474, SKBR3), medium (JIMT-1) and low HER2 density (MCF-7) cell lines studied using Incucyte live-cell imaging.

Table 3. IC_{50} of antibodies and ADCs in HER2-positive cell lines compared with T-DM1.

IC_{50} (nM)	BT-474	JIMT-1	MCF-7	SKBR3
T-DM1	59.9 ± 8.4	4.5 ± 0.5	135.6 ± 14.6	2.5 ± 2.3
Trastuzumab-PEG$_6$-DM1	44.3 ± 4.8	1.7 ± 0.7	89.8 ± 28.3	0.5 ± 0.7
Pertuzumab-PEG$_6$-DM1	41.3 ± 6.2	1.1 ± 0.2	15.9 ± 1.5	0.0036 ± 0.007
Trastuzumab-PEG$_6$-DM1 + pertuzumab-PEG$_6$-DM1	22.8 ± 3.2	0.2 ± 0.1	10.4 ± 1.6	0.0035 ± 0.006

Table 4. Pharmacokinetics parameters (mean ± SEM) of [^{89}Zr]Zr-trastuzumab-PEG$_6$-DM1 and [^{67}Cu]Cu-pertuzumab-PEG$_6$-DM1 in healthy Balb/c mice.

Construct	half-life $t_{1/2}$ α (h)	half-life $t_{1/2\beta}$ (h)	AUC (%IA h/mL)	Vss (mL)	CL (mL/h) × 10^{-3}
[^{89}Zr]Zr-trastuzumab-PEG$_6$-DM1	30.2 ± 18.6	431.0 ± 136.7	20175.5 ± 5405.0	2.8 ± 0.2	6 ± 1.3
[^{67}Cu]Cu-pertuzumab-PEG$_6$-DM1	6.4 ± 1.7	121.9 ± 18.6	4055.0 ± 392.0	4.1 ± 0.4	25 ± 2.7

Supplementary Fig. 5). The AUC (μm^2 h) of trastuzumab-PEG$_6$-DM1 was 32% ($P < 0.05$) greater than trastuzumab (Table 2). Similarly, the AUC of pertuzumab-PEG$_6$-DM1 was 38% greater than pertuzumab. The 1:1 combination of pertuzumab-PEG$_6$-DM1 and trastuzumab-PEG$_6$-DM1 led to further enhancement of the internalisation of the ADCs compared with the mono-incubation using the individual ADCs with up to 80% enhancement in internalisation compared with trastuzumab-PEG$_6$-DM1 (Table 2). In MCF-7 cells with the lowest HER2 expression, a similar difference between naked antibody and ADCs was observed. However, significant enhancement of internalisation of the biparatopic pertuzumab-PEG$_6$-DM1 + trastuzumab-PEG$_6$-DM1 was not observed with low HER2 density MCF-7 cell line (Supplementary Fig. 5A, B and Supplementary Table 3). These effects are delineated in the phase contrast images (Supplementary Fig. 6).

Novel ADC trastuzumab-PEG$_6$-DM1 was more potent ($P < 0.05$) than T-DM1 in BT-474, SKBR3, JIMT-1 and MCF-7 cell lines with IC_{50} of up to 3.5-fold lower (Fig. 4 and Table 3). As well, the IC_{50} of pertuzumab-PEG$_6$-DM1 was lower than ($P < 0.05$) trastuzumab-PEG$_6$-DM1 in all cell lines. The IC_{50} of biparatopic 1:1 combination of pertuzumab-PEG$_6$-DM1 + trastuzumab-PEG$_6$-DM1 were lower ($P < 0.05$) than for the treatment using the single agent pertuzumab-PEG$_6$-DM1 or trastuzumab-PEG$_6$-DM1 in all cell lines. Phase contrast images show enhanced uptake of cytotoxicity red dye indicative of cell death (Supplementary Fig. 7).

Stability and pharmacokinetics

The radioimmunoconjugates [^{89}Zr]Zr-trastuzumab-PEG$_6$-DM1 and [^{67}Cu]Cu-pertuzumab-PEG$_6$-DM1 were stable in human serum and PBS following incubation at 37 °C for 5 days (Supplementary Fig. 8). In vivo stability of [^{89}Zr]Zr-trastuzumab-PEG$_6$-DM1 and [^{67}Cu]Cu-pertuzumab-PEG$_6$-DM1 was performed in healthy Balb/c mice ($n = 3$).

Blood clearance of [^{67}Cu]Cu-pertuzumab-PEG$_6$-DM1 was faster than that of [^{89}Zr]Zr-trastuzumab-PEG$_6$-DM1 (Table 4 and Supplementary Fig. 9). The AUC of [^{67}Cu]Cu-pertuzumab-PEG$_6$-DM1 was twofold less than that of [^{89}Zr]Zr-trastuzumab-PEG$_6$-DM1. [^{89}Zr]Zr-trastuzumab-PEG$_6$-DM1 and [^{67}Cu]Cu-pertuzumab-PEG$_6$-DM1 displayed a biphasic clearance shown by a fast distribution (low $t_{1/2\alpha}$) and a slow clearance (high $t_{1/2\beta}$).

ImmunoPET/SPECT/CT imaging and biodistribution

ImmunoPET imaging using [^{89}Zr]Zr-trastuzumab-PEG$_6$-DM1, [^{89}Zr]Zr-rituximab-PEG$_6$-DM1, and immunoSPECT imaging using [^{67}Cu]

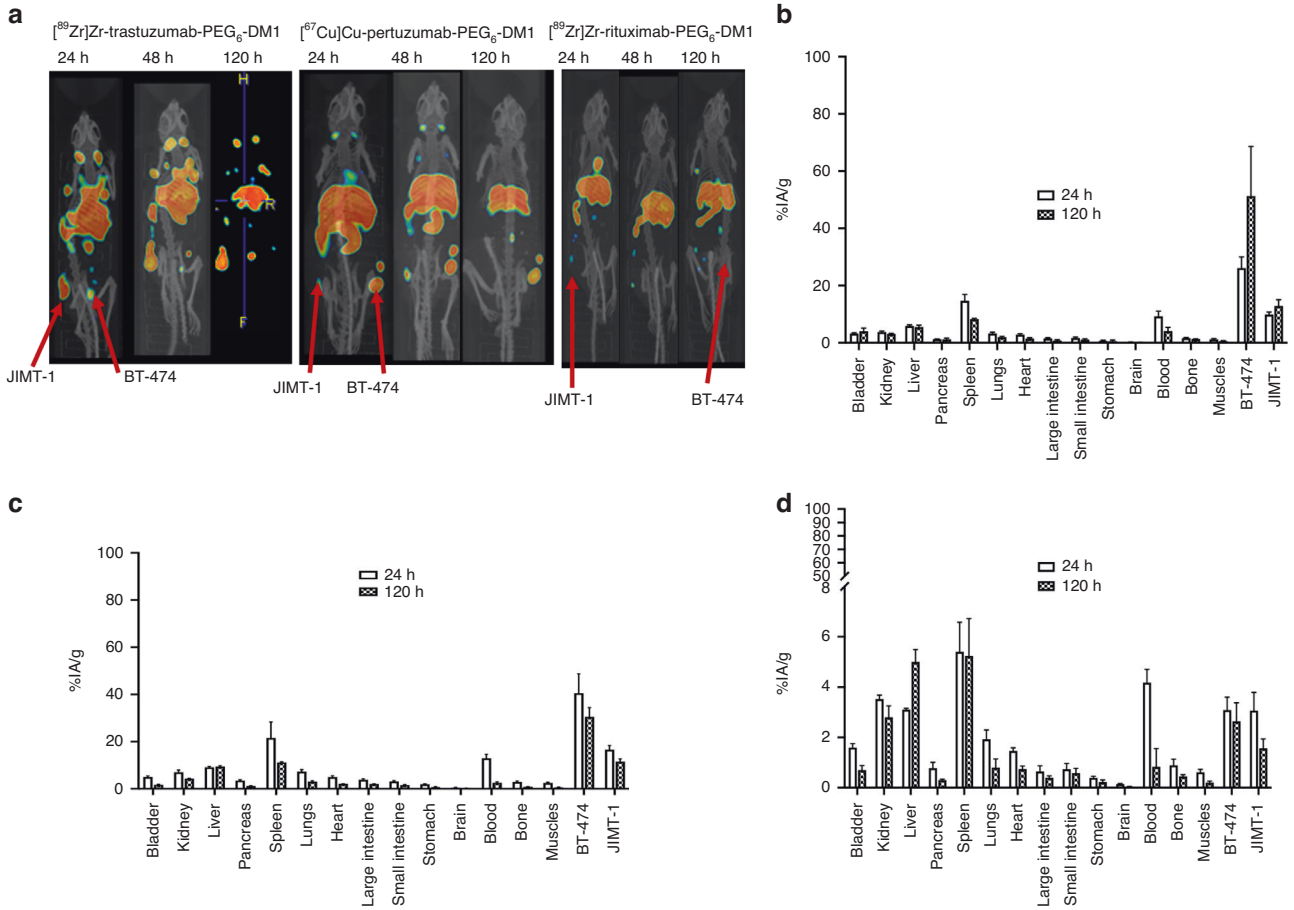

Fig. 5 MicroPET/SPECT/CT and biodistribution of antibody–drug radioconjugates at different timepoints post injection. a Molecular imaging of HER2 positive xenografts using [^{89}Zr]Zr-trastuzumab-PEG$_6$-DM1, [^{67}Cu]Cu-pertuzumab-PEG$_6$-DM1 and control immunoconjugate [^{89}Zr]Zr-rituximab-PEG$_6$-DM1 in CD-1 nude mice bearing HER2-positive JIMT-1 and BT-474 at different timepoints post injection. Biodistribution of athymic Balb/C nude mice bearing HER2-positive BT-474 and JIMT-1 xenografts following administration of **b** [^{89}Zr]Zr-trastuzumab-PEG$_6$-DM1, **c** [^{67}Cu]Cu-pertuzumab-PEG$_6$-DM1 and **d** Control [^{89}Zr]Zr-rituximab-PEG$_6$-DM1.

Cu-pertuzumab-PEG$_6$-DM1 in BT-474 (high HER2 expression), and JIMT-1 (medium HER2 expression) tumour xenografts were done at 24 h, 48 h and 120 h p.i. (Fig. 5a). Tumour uptake of [^{89}Zr]Zr-trastuzumab-PEG$_6$-DM1, [^{67}Cu]Cu-pertuzumab-PEG$_6$-DM1 and [^{89}Zr]Zr-rituximab-PEG$_6$-DM1 was also quantified by gamma counting following biodistribution studies (Fig. 5b–d). Tumour uptake of [^{67}Cu]Cu-pertuzumab-PEG$_6$-DM1 in athymic Balb/C nude mice bearing JIMT-1 and BT-474 decreased slightly (not significant) from 40.5 ± 8.2% IA/g at 24 h p.i. to 30.5 ± 3.9% IA/g at 120 h p.i. for BT-474 ($P = 0.9897$), and from 16.5 ± 1.8% IA/g (24 h) to 11.5 ± 1.2% IA/g at 120 h p.i. for JIMT-1 ($P > 0.9999$). On the other hand, for mice injected with [^{89}Zr]Zr-trastuzumab-PEG$_6$-DM1, tumour uptake at 24 h was 26.1 ± 3.9 % IA/g for BT-474, and 9.8 ± 0.9% IA/g for JIMT-1 which increased after 120 h to 51.3 ± 17.3% IA/g for BT-474 (P value = 0.4174) and 12.9 ± 2.1% IA/g for JIMT-1 (P value >0.9999). Low tumour uptake was observed in mice with control [^{89}Zr]Zr-rituximab-PEG$_6$-DM1 and was 3.1 ± 0.5% IA/g for BT-474 and 3.1 ± 0.7% IA/g for JIMT-1 at 24 h p.i. and 2.6 ± 0.7% IA/g for BT-474 and 1.6 ± 0.4% IA/g for JIMT-1 at 120 h confirming low nonspecific uptake of the conjugate.

Simultaneous targeting of domain IV and domain II was also studied following co-administration of [^{89}Zr]Zr-trastuzumab-PEG$_6$-DM1 and [^{67}Cu]Cu-pertuzumab-PEG$_6$-DM1 in athymic CD-1 nude mice bearing BT-474 and JIMT-1 xenografts using microSPECT/PET/CT. Tumours were simultaneously delineated using [^{89}Zr]Zr-trastuzumab-PEG$_6$-DM1 and [^{67}Cu]Cu-pertuzumab-PEG$_6$-DM1 (Fig. 6a, b). Similarly, a group of mice ($n = 3$) was pre-blocked using pertuzumab prior to administration of [^{89}Zr]Zr-trastuzumab-PEG$_6$-DM1, tumour uptake increased from 22.8 ± 8.2% IA/g at 24 h p.i. to 66.33 ± 33.9 % IA/g at 120 h p.i. for BT-474 (P value = 0.7233), and from 10.5 ± 2.4% IA/g at 24 h p.i. to 25.3 ± 4.9% IA/g at 120 h p.i. for JIMT-1 (P value >0.9999) (Fig. 6c). This shows specific uptake of [^{89}Zr]Zr-trastuzumab-PEG$_6$-DM1 and [^{67}Cu]Cu-pertuzumab-PEG$_6$-DM1 to HER2 expressing cell lines.

DISCUSSION

There have been significant advances in the treatment of HER2-positive BC, including the approvals of monoclonal antibodies (trastuzumab, pertuzumab, margetuximab and combinations), tyrosine kinase inhibitors (tucatinib, lapatinib), and ADCs (T-DM1 and T-DXd) [38]. Despite the initial benefits seen in patients with these agents, resistance is widespread. The addition of trastuzumab to taxanes chemotherapy increases the objective response rate (ORR) from 12 to 34%. However, de novo or acquired resistance is common in 66–88% of patients [39, 40]. ADCs are more potent than naked antibodies thanks to the cytotoxic payload. T-DXd is a second generation of anti-HER2 ADCs made up of a tetrapeptide-based linker and a cytotoxic topoisomerase I inhibitor with ORR of 60.9% in BC patients [38]. However, ADCs are also subjected to different acquired and de novo resistance mechanisms. Payload related mechanism include altered internalisation via caveolae-mediated endocytosis, altered lysosomal

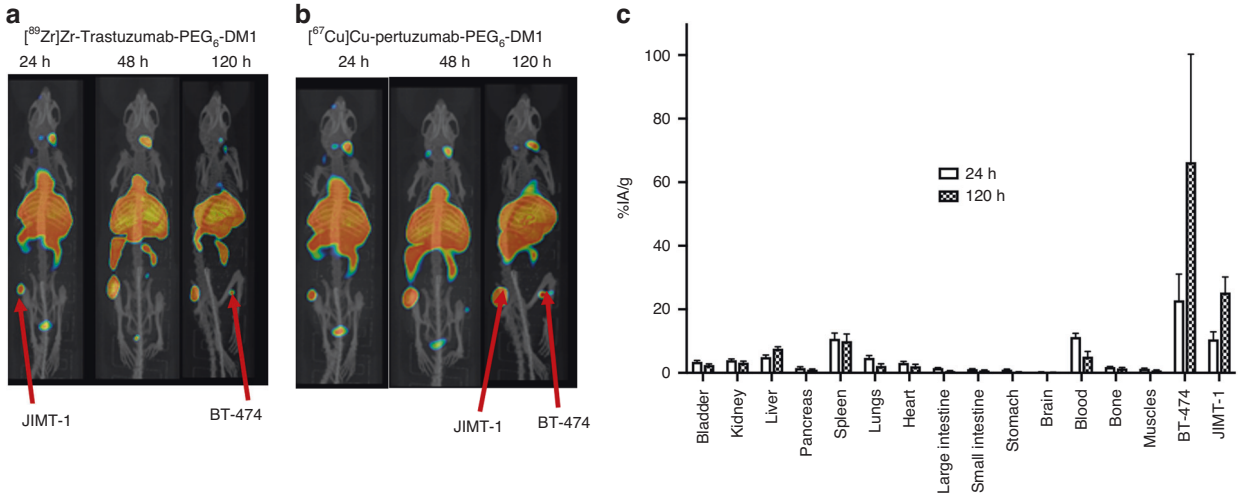

Fig. 6 Targeted antibody drug radioconjugate-specific imaging of HER2-positive xenografts following simultaneous injection of [^{89}Zr]Zr-trastuzumab-PEG$_6$-DM1 + [^{67}Cu]Cu-pertuzumab-PEG$_6$-DM1. Channels specific for gamma photons corresponding to ^{89}Zr ([^{89}Zr]Zr-trastuzumab-PEG$_6$-DM1 is represented in (**a**) and ^{67}Cu ([^{67}Cu]Cu-pertuzumab-PEG$_6$-DM1) is represented in (**b**). **c** Biodistribution of athymic Balb/C nude mice bearing HER2-positive BT-474 and JIMT-1 xenografts pre-injected using pertuzumab prior to administration of [^{89}Zr]Zr-trastuzumab-PEG$_6$-DM1.

acidification, hence no transport of the payload from the lysosomes to the cytoplasm, and mostly the extracellular efflux of the payload by membrane efflux transporters such as multidrug resistance (MDR) pumps [41, 42]. The use of alternative linker-payload chemistry, and combination therapies are potential ways to overcome resistance and increase response rates [43]. DM1 is the drug of choice for many ADCs including approved anti-HER2 T-DM1. Like most small-molecule chemotherapeutic agents, DM1 is an MDR1 substrate, however, PEGylated DM1 (PEG-DM1), as used in this study, has the same potency as DM1 but is not a substrate for MDR1 [25, 26]. Recently, Hartimath et al. demonstrated the efficacy of anti-EGFR ADC nimotuzumab-PEG$_6$-DM1 [32]. In addition, PEGylation improves drug solubility, and stability, decreases proteolysis and improves renal excretion and pharmacokinetics [44]. To the best of our knowledge this represents the first time trastuzumab-PEG$_6$-DM1, and pertuzumab-PEG$_6$-DM1 ADCs have been reported in the literature. In anticipation of future in vivo therapeutic efficacy studies of these two domain-specific ADCs in mouse models of HER2-positive BC, this study was undertaken to develop these agents, and to characterise their in vitro and in vivo behaviours using molecular imaging, as well as evaluate their in vitro cytotoxicity.

Our isotopes of choice to evaluate these ADCs in vivo were ^{89}Zr and ^{67}Cu because of their excellent decay characteristics, availability, and the fact that their physical half-lives; 78.4 h for ^{89}Zr and 61.8 h for ^{67}Cu match the biological half-lives of the IgGs. We produced trastuzumab-PEG$_6$-DM1 and pertuzumab-PEG$_6$-DM1 with average DAR of 3. As expected, conjugation of PEG$_6$-DM1 and bifunctional chelators decreased the binding of trastuzumab and pertuzumab to HER2. However, binding of the radiolabeled [^{89}Zr]Zr-trastuzumab-PEG$_6$-DM1 and [^{67}Cu]Cu-pertuzumab-PEG$_6$-DM1 was not significantly different from their naked antibodies. Trastuzumab and pertuzumab bind to different domains of HER2 as confirmed by the competitive binding assays using BT-474 [45, 46].

We evaluated the in vitro cytotoxicity of T-DM1, trastuzumab-PEG$_6$-DM1, pertuzumab-PEG$_6$-DM1 and the combination trastuzumab-PEG$_6$-DM1 + pertuzumab-PEG$_6$-DM1 in cells with different HER2 densities including a T-DM1 non-responsive cell line JIMT-1. Trastuzumab-PEG$_6$-DM1 and, pertuzumab-PEG$_6$-DM1 were more potent than T-DM1 in all cell lines. In addition, pertuzumab-PEG$_6$-DM1 was the most potent of the three ADCs, likely due to its highest internalisation rate and hence processing of the cytotoxin PEG$_6$-DM1. The combination of trastuzumab-PEG$_6$-DM1 + pertuzumab-PEG$_6$-DM1 was more potent than treatment using individual ADCs which was the result of increased internalisation of the domain-specific/biparatopic ADCs. In addition, biparatopic ADCs have been shown to cause enhanced receptor clustering and internalisation of the cytotoxic payloads resulting in enhanced cytotoxicity [22].

Pharmacokinetics is one of the critical attributes that affects the therapeutic index (toxicity versus efficacy) of the immunoconjugates. The elimination half-life ($t_{1/2\beta}$) of [^{89}Zr]Zr-trastuzumab-PEG$_6$-DM1 was 431.0 ± 136.7 h. In previous work, the elimination half-life of [^{89}Zr]Zr-nimotuzumab was 127.1 h in normal female mice [37]. We observed similar pharmacokinetic profiles for [^{67}Cu]Cu-pertuzumab-PEG$_6$-DM1 compared with [^{64}Cu]Cu-NOTA-trastuzumab as shown by Woo *et al.* in healthy mice [47]. The AUC of [^{89}Zr]Zr-trastuzumab-PEG$_6$-DM1 was almost five times higher (20175 vs 4055% IA.h/mL) than that of [^{67}Cu]Cu-pertuzumab-PEG$_6$-DM1. This is reflected in the fact that tumour uptake in both JIMT-1 and BT-474, particularly at later time (120 h p.i.) was higher for trastuzumab ADC than for the pertuzumab ADC, since the larger AUC results in an enhanced permeation and retention (EPR) effect similar to what is observed for other macromolecules. This observation is critical in the evaluation of the effectiveness of a biparatopic combination of both ADCs. Assuming a favourable toxicity trade-off, an increasing dose of pertuzumab-PEG$_6$-DM1 could result in a better combination index and therefore enhanced synergy [48, 49]. This will be tested in vivo.

Biparatopic targeting of antigens on cancer cells using antibodies enhances tumour cell clustering and receptor/antibody internalisation has shown some promise preclinically. Novel anti-HER2 and anti-EGFR biparatopic antibodies are currently under clinical development [22, 50]. Biparatopic SYM004 is a combination of two anti-EGFR antibodies (futuximab and modotuximab) that target different epitopes of domain III and it is in clinical trials for colorectal cancer [50, 51]. In preclinical mouse models, SYM004 showed superior activity compared with the single antibodies in cetuximab sensitive and insensitive models. Antibody internalisation, biodistribution and imaging data suggest that the presence of pertuzumab enhanced the internalisation and tumour uptake of [^{89}Zr]Zr-trastuzumab-PEG$_6$-DM1. When pertuzumab was administered prior to the injection of [^{89}Zr]Zr-trastuzumab-PEG$_6$-DM1 in mice bearing BT-474 and JIMT-1 xenografts tumour bearing mice, tumour uptake was higher

compared with no co-injection of pertuzumab. At 120 h p.i. tumour uptake of [^{89}Zr]Zr-trastuzumab-PEG$_6$-DM1 + pertuzumab was 66.33%IA/g (BT-474) and 25.3%IA/g (JIMT-1) compared with 51.3%IA/g (BT-474) and 12.9%IA/g (JIMT-1) when [^{89}Zr]Zr-trastuzumab-PEG$_6$-DM1 was administered without pertuzumab. Similarly, Al-Saden et al. showed that uptake of [^{89}Zr]Zr-labelled T-DM1® ([^{89}Zr]Zr-T-DM1) was 4.1-fold higher than [^{89}Zr]Zr-trastuzumab in BT-474 xenograft [52]. Our data corroborate those of Marquez et al. who showed that in the presence of trastuzumab, uptake of [^{89}Zr]Zr-pertuzumab was a few folds higher in HER2-positive xenografts [53].

CONCLUSION

To the best of our knowledge, our work is the first to use both [^{89}Zr]Zr-trastuzumab-PEG$_6$-DM1, and [^{67}Cu]Cu-pertuzumab-PEG$_6$-DM1 simultaneously as imaging tracers. The exciting possible synergistic or additive effect of these biparatopic immunoconjugates (trastuzumab-PEG$_6$-DM1 + pertuzumab-PEG$_6$-DM1) in vitro and in vivo holds promise for their use as a novel therapeutic approach. In addition, PEG$_6$-DM1 ADCs as opposed to DM1, either using the single agents or biparatopically could be more effective in BC patients that are refractory for T-DM1. In ongoing studies, we are evaluating this approach in mouse models of HER2-positive cancers.

DATA AVAILABILITY

The data that support the findings of this study are available from the corresponding author upon reasonable request.

REFERENCES

1. Canadian Cancer Statistics Advisory Committee in collaboration with the Canadian Cancer Society SCatPHAoC. Canadian Cancer Statistics 2021; 2021.
2. Latta EK, Tjan S, Parkes RK, O'Malley FP. The role of HER2/neu overexpression/amplification in the progression of ductal carcinoma in situ to invasive carcinoma of the breast. Mod Pathol. 2002;15:1318–25.
3. Gote V, Nookala AR, Bolla PK, Pal D. Drug resistance in metastatic breast cancer: tumor targeted nanomedicine to the rescue. Int J Mol Sci. 2021;22:4673.
4. Slamon DJ, Leyland-Jones B, Shak S, Fuchs H, Paton V, Bajamonde A, et al. Use of chemotherapy plus a monoclonal antibody against HER2 for metastatic breast cancer that overexpresses HER2. N Engl J Med. 2001;344:783–92.
5. Jahanzeb M. Adjuvant trastuzumab therapy for HER2-positive breast cancer. Clin Breast Cancer. 2008;8:324–33.
6. Wolff AC, Hammond ME, Schwartz JN, Hagerty KL, Allred DC, Cote RJ, et al. American Society of Clinical Oncology/College of American Pathologists guideline recommendations for human epidermal growth factor receptor 2 testing in breast cancer. J Clin Oncol. 2007;25:118–45.
7. Harris LN, You F, Schnitt SJ, Witkiewicz A, Lu X, Sgroi D, et al. Predictors of resistance to preoperative trastuzumab and vinorelbine for HER2-positive early breast cancer. Clin Cancer Res. 2007;13:1198–207.
8. Loibl S, Jackisch C, Schneeweiss A, Schmatloch S, Aktas B, Denkert C, et al. Dual HER2-blockade with pertuzumab and trastuzumab in HER2-positive early breast cancer: a subanalysis of data from the randomized phase III GeparSepto trial. Ann Oncol. 2017;28:497–504.
9. von Minckwitz G, Procter M, de Azambuja E, Zardavas D, Benyunes M, Viale G, et al. Adjuvant pertuzumab and trastuzumab in early HER2-positive breast cancer. N Engl J Med. 2017;377:122–31.
10. Nami B, Maadi H, Wang Z. Mechanisms underlying the action and synergism of trastuzumab and pertuzumab in targeting HER2-positive breast cancer. Cancers. 2018;10:342.
11. Tsao L-C, Crosby EJ, Trotter TN, Wei J, Wang T, Yang X, et al. Trastuzumab/pertuzumab combination therapy stimulates antitumor responses through complement-dependent cytotoxicity and phagocytosis. JCI Insight. 2022;7:e155636.
12. Richard S, Selle F, Lotz J-P, Khalil A, Gligorov J, Soares DG. Pertuzumab and trastuzumab: the rationale way to synergy. An da Academia Brasileira de Ciências. 2016;88:565–77.
13. Verma S, Miles D, Gianni L, Krop IE, Welslau M, Baselga J, et al. Trastuzumab emtansine for HER2-positive advanced breast cancer. N Engl J Med. 2012;367:1783–91.
14. Lewis Phillips GD, Li G, Dugger DL, Crocker LM, Parsons KL, Mai E, et al. Targeting HER2-positive breast cancer with trastuzumab-DM1, an antibody-cytotoxic drug conjugate. Cancer Res. 2008;68:9280–90.
15. Junutula JR, Flagella KM, Graham RA, Parsons KL, Ha E, Raab H, et al. Engineered thio-trastuzumab-DM1 conjugate with an improved therapeutic index to target human epidermal growth factor receptor 2-positive breast cancer. Clin Cancer Res. 2010;16:4769–78.
16. Barok M, Joensuu H, Isola J. Trastuzumab emtansine: mechanisms of action and drug resistance. Breast Cancer Res. 2014;16:209.
17. Shefet-Carasso L, Benhar I. Antibody-targeted drugs and drug resistance-challenges and solutions. Drug Resist Updat. 2015;18:36–46.
18. Singh AP, Sharma S, Shah DK. Quantitative characterization of in vitro bystander effect of antibody-drug conjugates. J Pharmacokinet Pharmacodyn. 2016;43:567–82.
19. Modi S, Saura C, Yamashita T, Park YH, Kim SB, Tamura K, et al. Trastuzumab deruxtecan in previously treated HER2-positive breast cancer. N Engl J Med. 2020;382:610–21.
20. Keam SJ. Trastuzumab deruxtecan: first approval. Drugs. 2020;80:501–8.
21. Ogitani Y, Hagihara K, Oitate M, Naito H, Agatsuma T. Bystander killing effect of DS-8201a, a novel anti-human epidermal growth factor receptor 2 antibody-drug conjugate, in tumors with human epidermal growth factor receptor 2 heterogeneity. Cancer Sci. 2016;107:1039–46.
22. Li JY, Perry SR, Muniz-Medina V, Wang X, Wetzel LK, Rebelatto MC, et al. A biparatopic HER2-targeting antibody-drug conjugate induces tumor regression in primary models refractory to or ineligible for HER2-targeted therapy. Cancer Cell. 2016;29:117–29.
23. Comer F, Gao CS, Coats S. Bispecific and biparatopic antibody drug conjugates. Cancer Drug Discov D. Cham; Springer International Publishing. 2018. p. 267–80.
24. Hamblett KJ, Barnscher SD, Davies RH, Hammond PW, Hernandez A, Wickman GR, et al. ZW49, a HER2 targeted biparatopic antibody drug conjugate for the treatment of HER2 expressing cancers. Cancer Res. 2018;78:3914.
25. Kovtun YV, Audette CA, Mayo MF, Jones GE, Doherty H, Maloney EK, et al. Antibody-maytansinoid conjugates designed to bypass multidrug resistance. Cancer Res. 2010;70:2528–37.
26. Zhao RY, Wilhelm SD, Audette C, Jones G, Leece BA, Lazar AC, et al. Synthesis and evaluation of hydrophilic linkers for antibody-maytansinoid conjugates. J Med Chem. 2011;54:3606–23.
27. Henry KE, Ulaner GA, Lewis JS. Human epidermal growth factor receptor 2-targeted PET/single-photon emission computed tomography imaging of breast cancer: noninvasive measurement of a biomarker integral to tumor treatment and prognosis. PET Clin. 2017;12:269–88.
28. Keinänen O, Fung K, Brennan JM, Zia N, Harris M, Van Dam E, et al. Harnessing64Cu/67Cu for a theranostic approach to pretargeted radioimmunotherapy. Proc Natl Acad Sci USA. 2020;117:28316–27.
29. Hao G, Mastren T, Silvers W, Hassan G, Öz OK, Sun X. Copper-67 radioimmunotheranostics for simultaneous immunotherapy and immuno-SPECT. Sci Rep. 2021;11:1–11.
30. Liang Y, Besch-Williford C, Hyder SM. PRIMA-1 inhibits growth of breast cancer cells by re-activating mutant p53 protein. Int J Oncol. 2009;35:1015–23.
31. Hartimath SV, Alizadeh E, Solomon VR, Chekol R, Bernhard W, Hill W, et al. Preclinical evaluation of (111)In-labeled PEGylated maytansine nimotuzumab drug conjugates in EGFR-positive cancer models. J Nucl Med. 2019;60:1103–10.
32. Hartimath SV, El-Sayed A, Makhlouf A, Bernhard W, Gonzalez C, Hill W, et al. Therapeutic potential of nimotuzumab PEGylated-maytansine antibody drug conjugates against EGFR positive xenograft. Oncotarget. 2019;10:1031–44.
33. Chen Y. Drug-to-antibody ratio (DAR) by UV/Vis spectroscopy. Totowa, NJ: Humana Press; 2013. p. 267–73.
34. Tikum AF, Nambisan AK, Ketchemen JP, Babeker H, Khan MN, Torlakovic EE, et al. Simultaneous imaging and therapy using epitope-specific anti-epidermal growth factor receptor (EGFR) antibody conjugates. Pharmaceutics. 2022;14:1917.
35. Solomon VR, Barreto K, Bernhard W, Alizadeh E, Causey P, Perron R, et al. Nimotuzumab site-specifically labeled with 89Zr and 225Ac using SpyTag/SpyCatcher for PET imaging and alpha particle radioimmunotherapy of epidermal growth factor receptor positive cancers. Cancers. 2020;12:3449.
36. Alizadeh E, Behlol Ayaz Ahmed K, Raja Solomon V, Gaja V, Bernhard W, Makhlouf A, et al. (89)Zr-labeled domain II-specific scFv-Fc immunoPET probe for imaging epidermal growth factor receptor in vivo. Cancers. 2021;13:560.
37. Chekol R, Solomon VR, Alizadeh E, Bernhard W, Fisher D, Hill W, et al. (89)Zr-nimotuzumab for immunoPET imaging of epidermal growth factor receptor I. Oncotarget. 2018;9:17117–32.
38. Ferrario C, Christofides A, Joy AA, Laing K, Gelmon K, Brezden-Masley C. Novel therapies for the treatment of HER2-positive advanced breast cancer: a Canadian perspective. Curr Oncol. 2022;29:2720–34.

39. Swain SM, Baselga J, Kim S-B, Ro J, Semiglazov V, Campone M, et al. Pertuzumab, trastuzumab, and docetaxel in HER2-positive metastatic breast cancer. N Engl J Med. 2015;372:724–34.
40. Zhang X, Chen J, Weng Z, Li Q, Zhao L, Yu N, et al. A new anti-HER2 antibody that enhances the anti-tumor efficacy of trastuzumab and pertuzumab with a distinct mechanism of action. Mol Immunol. 2020;119:48–58.
41. Vernieri C, Milano M, Brambilla M, Mennitto A, Maggi C, Cona MS, et al. Resistance mechanisms to anti-HER2 therapies in HER2-positive breast cancer: current knowledge, new research directions and therapeutic perspectives. Crit Rev Oncol/Hematol. 2019;139:53–66.
42. Luque-Bolivar A, Pérez-Mora E, Villegas VE, Rondón-Lagos M. Resistance and overcoming resistance in breast cancer. Breast Cancer: Targets Ther. 2020;12:211–29.
43. Hunter FW, Barker HR, Lipert B, Rothé F, Gebhart G, Piccart-Gebhart MJ, et al. Mechanisms of resistance to trastuzumab emtansine (T-DM1) in HER2-positive breast cancer. Br J Cancer. 2020;122:603–12.
44. Veronese FM, Mero A. The impact of PEGylation on biological therapies. BioDrugs. 2008;22:315–29.
45. Massicano AVF, Lee S, Crenshaw BK, Aweda TA, El Sayed R, Super I, et al. Imaging of HER2 with [(89)Zr]pertuzumab in response to T-DM1 therapy. Cancer Biother Radiopharm. 2019;34:209–17.
46. Lam K, Chan C, Reilly RM. Development and preclinical studies of 64Cu-NOTA-pertuzumab F(ab′)2 for imaging changes in tumor HER2 expression associated with response to trastuzumab by PET/CT. mAbs. 2017;9:154–64.
47. Woo S-K, Jang SJ, Seo M-J, Park JH, Kim BS, Kim EJ, et al. Development of 64Cu-NOTA-trastuzumab for HER2 targeting: a radiopharmaceutical with improved pharmacokinetics for human studies. J Nucl Med. 2019;60:26–33.
48. Nair SK, Verma A, Thomas TJ, Chou TC, Gallo MA, Shirahata A, et al. Synergistic apoptosis of MCF-7 breast cancer cells by 2-methoxyestradiol and bis(ethyl) norspermine. Cancer Lett. 2007;250:311–22.
49. Chou TC. Theoretical basis, experimental design, and computerized simulation of synergism and antagonism in drug combination studies. Pharm Rev. 2006;58:621–81.
50. Sanchez-Martin FJ, Bellosillo B, Gelabert-Baldrich M, Dalmases A, Canadas I, Vidal J, et al. The first-in-class anti-EGFR antibody mixture Sym004 overcomes cetuximab resistance mediated by EGFR extracellular domain mutations in colorectal cancer. Clin Cancer Res. 2016;22:3260–7.
51. Montagut C, Argiles G, Ciardiello F, Poulsen TT, Dienstmann R, Kragh M, et al. Efficacy of Sym004 in patients with metastatic colorectal cancer with acquired resistance to anti-EGFR therapy and molecularly selected by circulating tumor DNA analyses: a phase 2 randomized clinical trial. JAMA Oncol. 2018;4:e175245.
52. Al-Saden N, Lam K, Chan C, Reilly RM. Positron-emission tomography of HER2-positive breast cancer xenografts in mice with 89Zr-labeled trastuzumab-DM1: a comparison with 89Zr-labeled trastuzumab. Mol Pharm. 2018;15:3383–93.
53. Marquez BV, Ikotun OF, Zheleznyak A, Wright B, Hari-Raj A, Pierce RA, et al. Evaluation of (89)Zr-pertuzumab in Breast cancer xenografts. Mol Pharm. 2014;11:3988–95.

ACKNOWLEDGEMENTS
The authors wish to acknowledge the contributions of Dr. Vijay Gaja (Canadian Isotope Innovations Corp CIIC) for providing [^{67}Cu]$CuCl_2$, and Dr. Musharraf Khan (Saskatchewan Cyclotron Facility) for assistance with experiments.

AUTHOR CONTRIBUTIONS
Experimental design, execution and data analysis were performed by JPK, HB, AFT, AKN, FNN, EN and HF. Writing of the original draft preparation and review were done by JPK and HF. All the authors contributed to the article and approved the submitted version.

FUNDING
This work was funded by Canadian Institute for Health Research (CIHR) Project Grants (# 437660 and 408132) to HF.

COMPETING INTERESTS
The authors declare no competing interests.

ETHICS APPROVAL AND CONSENT TO PARTICIPATE
All animal experiments were approved, supervised, and maintained following the guidelines of the University of Saskatchewan Animal Care Committee (UACC). Ethical approval references 20170084 and 20220021.

CONSENT FOR PUBLICATION
Not applicable.

ADDITIONAL INFORMATION
Supplementary information The online version contains supplementary material available at https://doi.org/10.1038/s41416-023-02272-4.

Correspondence and requests for materials should be addressed to Humphrey Fonge.

Reprints and permission information is available at http://www.nature.com/reprints

Publisher's note Springer Nature remains neutral with regard to jurisdictional claims in published maps and institutional affiliations.